Rare gas collisions with molten metal surfaces

W. W. Hayes and J. R. Manson[a)]
Department of Physics and Astronomy, Clemson University, Clemson, South Carolina 29634, USA

(Received 16 April 2007; accepted 20 August 2007; published online 29 October 2007)

Newly available experimental data for the scattering of argon, neon, and xenon atoms from molten gallium, indium, and bismuth surfaces are compared to calculations with classical scattering theory. The results of the theory are in reasonable agreement with observed energy-resolved spectra taken at fixed angles, with in-plane angular distributions, and with the first available out-of-plane angular distribution spectra for these systems. For all three of the rare gases, scattering from liquid Ga required the use of an effective surface mass equal to 1.65 times the mass of a single Ga atom. The need for a larger effective mass has been noted previously for Ar/Ga scattering and is indicative of collective effects in the liquid Ga. Comparisons with data taken at low incident energies enable estimates of the physisorption well depth in the interaction potentials for many of the gas-metal combinations. © *2007 American Institute of Physics*. [DOI: 10.1063/1.2786073]

I. INTRODUCTION

A recent paper reported extensive measurements of high-quality state-to-state scattering intensities for beams of three different rare gases colliding with molten metal surfaces.[1] The gas atoms were Ne, Ar, and Xe and the metals were Ga, In, and Bi. Previously, measurements on similar systems were presented for angular distributions and energy-resolved scattered spectra,[2–5] but the present measurements cover a wider range of initial experimental conditions and also include measurements of the scattering intensities out of the plane of scattering.

The purpose of this paper is to examine these new data in comparisons with calculations using a classical mechanical scattering theory that was successful in explaining many of the features of the earlier, more restricted, experimental results.[6–8] As in these previous studies, we find here that many of the observed features can be explained by classical scattering theory.

At very low incident beam energies, where adsorption into the physisorption well at the surface should become an important mechanism, it has been found that a significant portion of the scattered intensity in these and similar systems consists of initially trapped particles that are subsequently desorbed with an approximately equilibrium distribution.[1,2,9,10] The present theoretical analysis provides a means to estimate the adsorbed-desorbed fraction. Also, in the case of all data taken at low energies, a comparison with both angular distributions and energy-resolved spectra was substantially better when a physisorption well was included in the interaction potential, and this provides estimates of the well depths D for all gas-liquid combinations for which low-energy data were available.

For all three of the atomic probes, scattering from Ga behaved differently from that from In or Bi because it was necessary to use an effective mass larger than the mass of a single Ga atom in order to obtain a quantitative agreement with measurements. This larger effective mass implies a collective effect in which the gas atom interacts with a surface in which the underlying mass is, on average, larger than that of one metal atom. Such a conclusion is consistent with recent observations that Ga, even at high temperatures, retains unusually large vestiges of ordered layering near the surface.[11–14]

The organization of this paper is as follows: The theory is briefly described in the next section. Comparisons of calculations with the experimental measurements are presented and discussed in Sec. III, and some conclusions are presented in Sec. IV.

II. THEORY

The single-collision scattering of an atomic projectile from a smooth surface with vibrational corrugations caused by motions of the underlying substrate atoms can be solved in terms of closed-form expressions in the classical limit. The differential reflection coefficient, $dR(\mathbf{p}_f,\mathbf{p}_i)/d\Omega_f dE_f$, describing the probability of an incident beam of particles with momentum $\mathbf{p}_i$ being scattered into a final energy dE_f and solid angle $d\Omega_f$ intervals centered about momentum $\mathbf{p}_f$, is given by[15–17]

$$\frac{dR^{(1)}(\mathbf{p}_f,\mathbf{p}_i)}{d\Omega_f dE_f} = \frac{m^2 v_R^2 |\mathbf{p}_f|}{8\pi^3 \hbar^2 p_{iz} S_{uc}} |\tau_{fi}|^2 \left(\frac{\pi}{k_B T_S \Delta E_0}\right)^{3/2} \times \exp\left\{-\frac{(E_f - E_i + \Delta E_0)^2 + 2v_R^2 \mathbf{P}^2}{4k_B T_S \Delta E_0}\right\}, \quad (1)$$

where m is the projectile atomic mass, p_{iz} is the surface-normal component of the incident momentum, T_S is the temperature, k_B is Boltzmann's constant, the binary recoil energy is $\Delta E_0 = (\mathbf{p}_f - \mathbf{p}_i)^2/2M_C$, with M_C as the target substrate mass, $\mathbf{P}$ is the parallel component of the scattering vector $\mathbf{p}_f - \mathbf{p}_i$, and $|\tau_{fi}|^2$ is a form factor determined by the interaction potential. The factor S_{uc} is the surface area associated with a single surface atom and v_R is a parameter having dimensions of speed that is completely determined by the phonon spec-

a)Electronic mail: jmanson@clemson.edu

tral density at the classical turning point. As is usually the case, it is treated as a parameter here.[15,16] In a purely classical derivation of Eq. (1), $\hbar$ is a constant having dimensions of action, while if the same result is derived from quantum mechanical cross sections by taking the classical limit, it is identified as Planck's constant divided by 2π.

The case of multiple collisions of the incoming projectile with the surface can be treated as convolutions of successive single collisions. The differential reflection coefficient including both single and double scattering terms is

$$\frac{dR^{(2)}(\mathbf{p}_f,\mathbf{p}_i)}{d\Omega_f dE_f} = \frac{dR^{(1)}(\mathbf{p}_f,\mathbf{p}_i)}{d\Omega_f dE_f} + \left\langle \sum_{n=1}^{N} \int_0^\infty dE_q \int_{\Delta\Omega_n} d\Omega_q \frac{dR^{(1)}(\mathbf{p}_f,\mathbf{p}_q)}{d\Omega_f dE_f} \frac{dR^{(1)}(\mathbf{p}_q,\mathbf{p}_i)}{d\Omega_f dE_f} \right\rangle. \tag{2}$$

For a liquid, the angular brackets signify the average over the positions of the number N of neighboring surface atoms and $\Delta\Omega_n$ is the solid angle subtended by the second atom as viewed from the initial collision. For the calculations presented here, N includes the six nearest neighbor atoms in the surface plane.

Consistent with the approximations used to obtain Eq. (1), the form factor $|\tau_{fi}|^2$ is the transition matrix element for the elastic interaction potential extended off the energy shell, i.e., taken with respect to final and initial particle wave functions that do not have the same energies. If the repulsive part of the interaction potential is flat and strongly repulsive, then the leading term in the perturbation series for the matrix element is

$$\tau_{fi} = 4p_{fz}p_{iz}/m, \tag{3}$$

a limiting form that has been shown useful in previous studies of atom and molecule scattering from surfaces. Because the form factor, in the limit of Eq. (3), is the product of two functions—each involving only the initial or final state—it factors out of the multiple collision differential reflection coefficient of Eq. (1) and becomes an overall factor multiplying all terms.

When the incident energy is small, the physisorption well in the interaction potential, in addition to giving rise to trapping, has important effects on the scattering spectra. In this work, the physisorption potential is modeled by a square well potential of depth D. In the classical limit, a square well does an adequate job of describing the enhanced energy and refraction of the incident beam toward normal as the particles enter the physisorption potential. The width of the well is unimportant as long as it is larger than the normal displacements of the surface.

The double scattering term of Eq. (2) involves integrals over intermediate energies and angles. The intermediate solid angle is determined from the relation

$$\frac{\Delta\Omega_n}{4\pi} = \frac{\pi(a_1+a_2)^2}{4\pi d^2}, \tag{4}$$

where a_1 and a_2 are the radii of the projectile and substrate atoms and d is the average interatomic distance in the liquid metal. The differential reflection coefficient does not vary strongly over the area subtended by each of the second substrate atoms, so the angular integration is replaced by a multiplicative factor of $\Delta\Omega_n$. This approximation has been checked by carrying out exact integrations over intermediate angles, and differences in the final results were small.

In previous work analyzing rare gas scattering from molten metals, energy-resolved spectra were calculated using a different differential reflection coefficient, one that describes scattering from a discrete collection of scattering centers. In this work, all calculations, including the multiple scattering terms, are carried out with the smooth surface model of Eq. (1). The comparisons shown below for energy-resolved spectra include both single and double scattering contributions. All angular distributions, both in plane and out of plane, are calculated using only the single scattering term. This is because the angular distributions are integrated over all final energies and they are quite broad. Because of the energy integration, the calculated angular distributions do not differ appreciably in shape if the double scattering term is added or not; the major effect is a small increase in overall intensity. Because the double scattering contribution has little effect and because it is much more lengthy to calculate, the calculations of angular distributions were done with only the single-collision contribution.

Other points that should be mentioned involve particular details of the detector.[1] For all energy-resolved measurements, the probability of detection was proportional to the time spent passing through the detection volume, and the data were corrected for this.[1] For the angular distributions, a different detection apparatus was used, and there is no detector correction factor. The out-of-plane intensity measurements were made by rigidly translating the detector perpendicular to the scattering plane (i.e., the plane containing the incident beam and the normal to the surface). Thus, they are reported not in terms of the usual azimuthal angle of spherical coordinates, but instead in terms of an angle α which is measured perpendicularly to the scattering plane at the final in-plane polar angle θ_f.

III. COMPARISON WITH EXPERIMENT

A. Argon on gallium

A series of measured energy-resolved intensity spectra as functions of final energy for argon scattering from a liquid gallium surface at different temperatures was exhibited in Ref. 1, and an example is shown in Fig. 1. The detector is in

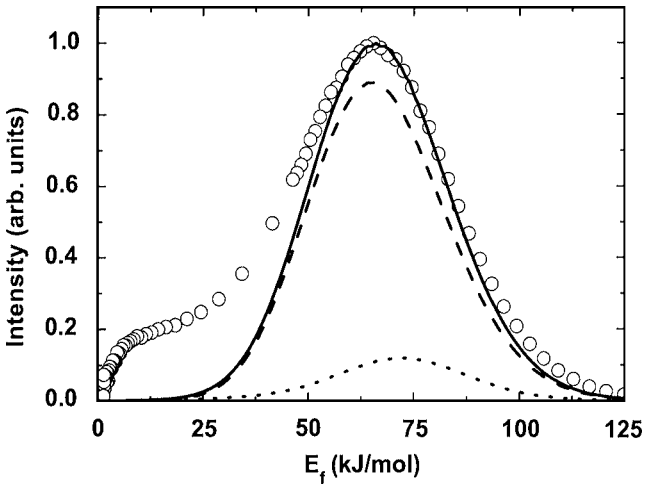

FIG. 1. Energy-resolved spectrum of Ar scattered from a liquid Ga surface with a temperature of 673 K, $\theta_i=\theta_f=55°$, and $E_i=95$ kJ/mol. Experimental data are circles, the total scattering calculation is the solid curve, the single scattering is the dashed curve, and the double scattering is the dotted curve.

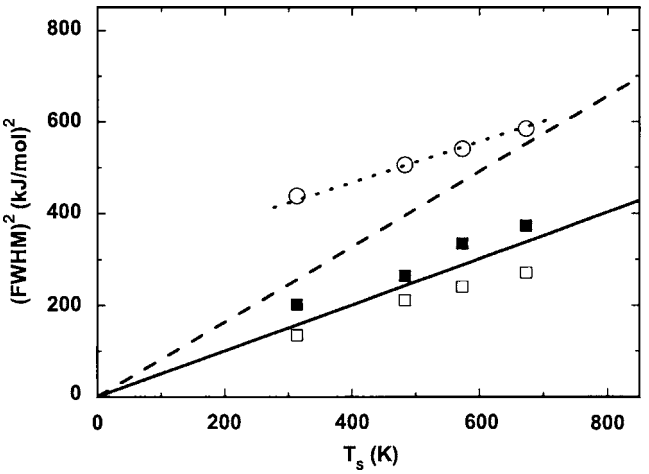

FIG. 2. Temperature dependence of the squared FWHM for Ar scattered from a liquid Ga surface with $\theta_i=\theta_f=55°$ and $E_i=95$ kJ/mol. The solid line (—) is the Gaussian approximation of Eq. (5) and the dashed line is the trajectory approximation. Data are circles, the calculated single scatterings are the open squares and the total scatterings are the solid squares. The dotted line is a linear fit to the total scattering (i.e., to the solid squares) with a constant offset added for comparison with the slope of the data.

the plane of scattering with equal incident and final polar angles $\theta_f=\theta_i=55°$, the incident energy is $E_i=95$ kJ/mol, and the surface temperatures range from 313 to 673 K. The spectra are characterized by a single broad, asymmetric peak with a very distinct shoulder at low energies and whose full width at half maximum (FWHM) increases with temperature. The peak position, or most probable final energy, is at about two-thirds of the incident energy, indicating a substantial average energy loss to the surface. Calculations using Eq. (2) are shown as the solid curve. This is the sum of the single-collision contribution of Eq. (1) shown as a dashed curve and the double collision contribution, which is smaller, shown as a dotted curve.

The low-energy shoulder evident in the data of Fig. 1 is not produced by the smooth-model multiple collision calculation used here because the form factor of Eq. (3) becomes too small at very low energies and suppresses this feature. This shoulder is due to double backscattering trajectories in which the incident particle is first scattered backwards nearly parallel to the surface and then is scattered forward into the detector by the second collision, as has been demonstrated by calculations based on hard-sphere scattering.[8]

The calculations show essentially no shift in the position of the most probable final energy with increasing temperature, in agreement with the experiment for which the position varies by no more than 2 kJ/mol over the whole range of temperatures measured. There is a marked increase in the width of the peak with increasing temperature, and this is discussed further below in connection with Fig. 2.

The value of $\Delta\Omega/4\pi$ used in the calculations was 0.162, which was calculated from Eq. (4) using the covalent radii of argon $a_{\mathrm{Ar}}=0.126$ nm and gallium $a_{\mathrm{Ga}}=0.098$ nm and an average interatomic spacing of $d=0.278$ nm for the liquid. The value of v_R was chosen to be 600 m/s for all calculations of the Ar/Ga system.

For calculations of all three rare gas probes on gallium, it was necessary to choose M_C to be an effective mass equal to 1.65 times the mass of a single Ga atom. The reason for this lies in the sensitivity of the most probable energy to M_C, and if a smaller effective mass is used the calculated most probable final energy becomes significantly smaller than that observed. This need for a larger effective mass with Ga contrasts with the In and Bi results treated below, where M_C was always chosen equal to the atomic mass of the liquid metal.

The temperature dependence of the FWHM for the energy-resolved spectra of Fig. 1 for Ar/Ga scattering is shown in Fig. 2. The data, shown as open circles, show the expected very nearly linear dependence of the squared FWHM with surface temperature. Both single and single plus double scattering calculations, shown as open and filled squares, respectively, show a similar linear dependence with nearly the same slope, but smaller by a constant value over the whole temperature range. The constant difference of about 300 $\mathrm{kJ}^2/\mathrm{mol}^2$ between experiment and calculations implies that this must be due to a mechanism that does not involve thermal processes; i.e., it is not due to phonons or low-energy electron-hole pair excitation.

The linear temperature dependence appearing in Fig. 2 can be readily extracted from Eq. (1). For initial conditions in which the term in $\mathbf{P}^2$ in the exponent of Eq. (1) is small, which is the case here, a Gaussian approximation to the single scattering gives the result

$$(\mathrm{FWHM})^2 \approx 16\ln(2)g(\theta)E_i k_B T_S, \tag{5}$$

where θ is the total scattering angle (the angle between $\mathbf{p}_f$ and $\mathbf{p}_i$) and

$$g(\theta) = \frac{g_{\mathrm{TA}}(\theta)}{[1+\mu-\mu\cos\theta/\sqrt{f(\theta)}]^2}, \tag{6}$$

with $g_{\mathrm{TA}}(\theta)$, the trajectory approximation to $g(\theta)$, given by

$$g_{\mathrm{TA}}(\theta) = \mu[1+f(\theta)-2\sqrt{f(\theta)}\cos(\theta)]. \tag{7}$$

The function

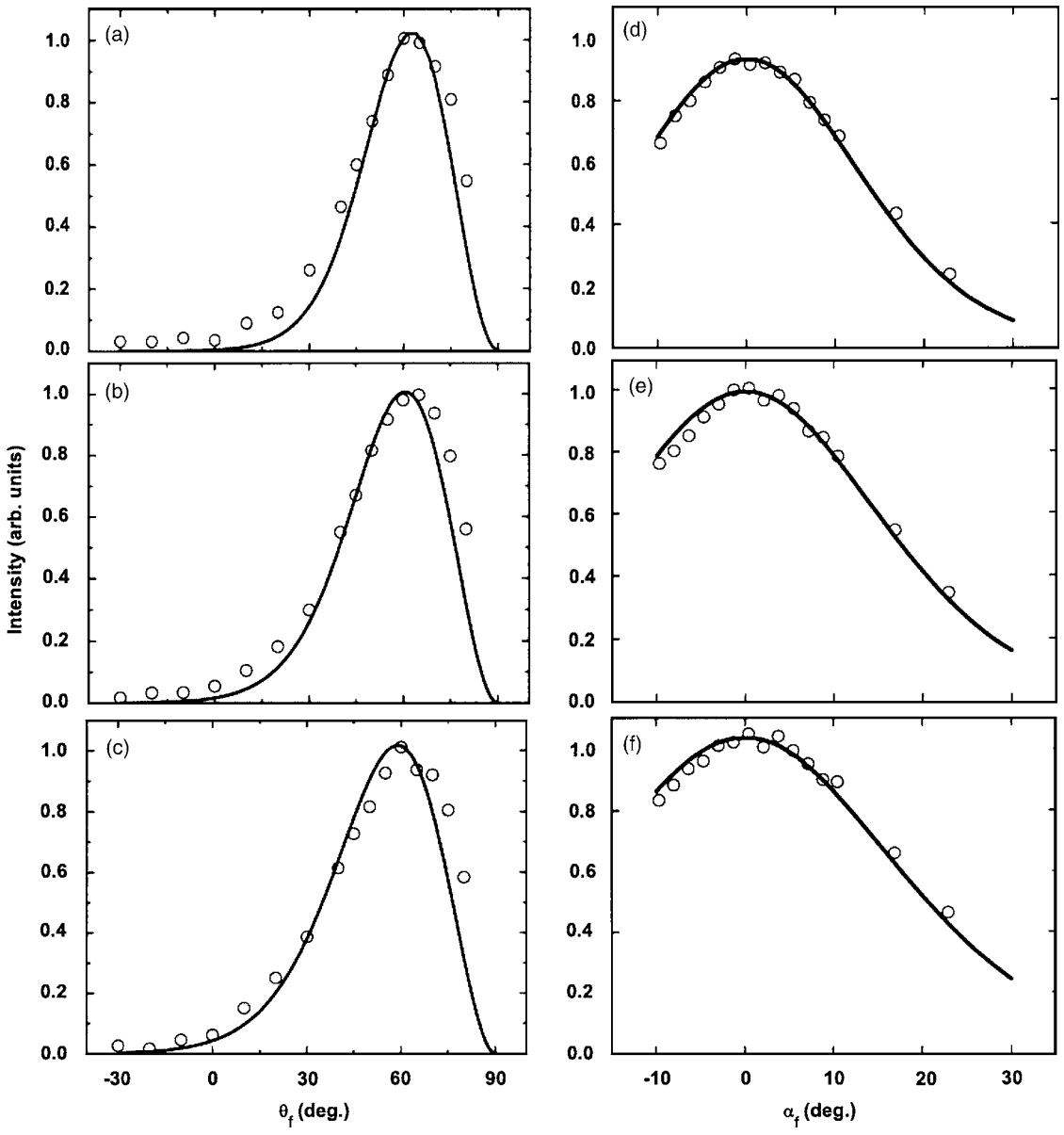

FIG. 3. In-plane (left panels) and out-of-plane (right panels) angular distributions for Ar/Ga with $\theta_i=55°$ and $E_i=92$ kJ/mol for three different values of surface temperature: [(a) and (d)] 308 K, [(b) and (e)] 436 K, and [(c) and (f)] 586 K. Data are circles and calculations are the solid curves.

$$f(\theta)=\left(\frac{\sqrt{1-\mu^2\sin^2\theta}+\mu\cos\theta}{1+\mu}\right)^2 \tag{8}$$

comes from setting $E_f-E_i+\Delta E_0=0$, which results in the Baule expression for the energy transfer in a hard-sphere collision $E_f=f(\theta)E_i$. For completeness, the approximation of Eq. (5) and the trajectory approximation are also shown in Fig. 2.

Angular distributions for Ar/Ga are shown in Fig. 3. These are compared with calculations, shown as solid curves, which are the integral of Eq. (1) over all final energies. Figure 3 shows both in-plane and out-of-plane angular distributions for an incident energy $E_i=92$ kJ/mol and $\theta_i=55°$ for three different surface temperatures ranging from 308 to 586 K. In this case, the good agreement between measurement and theory indicates that there is little or no diffuse equilibrium component in the scattering distributions because this would be expected to appear as a $\cos(\theta_f)$ contribution.

Figure 4 shows as open circles an in-plane angular distribution for Ar/Ga measured at a temperature of 586 K with an incident energy corresponding to a room temperature jet beam with $E_i=6$ kJ/mol and $\theta_i=55°$. In this case, the scattered intensity is spread over a much larger angular range, indicating that there is significant adsorption with subsequent desorption. It is usually assumed that the desorbed particles leave with the surface in equilibrium, and the filled circles are the same data with a fraction of a Knudsen equilibrium flux distribution subtracted, this fraction being equal to 43% at 308 K, 40% at 436 K, and 35% at 586 K. The solid curves are the calculations, which in this case include an attractive physisorption well of depth $D=60$ meV (5.8 kJ/mol). Although the agreement is not as good as for the higher energy

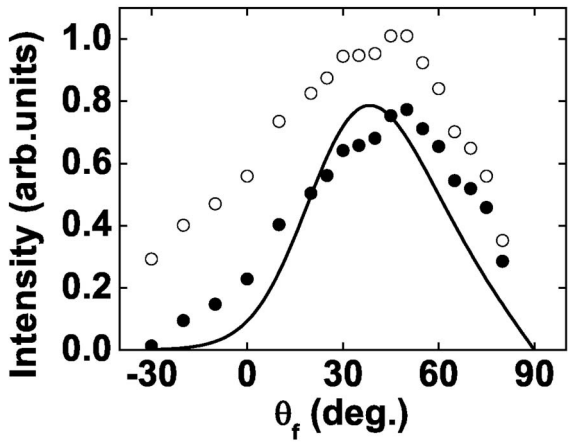

FIG. 4. In-plane angular distribution for Ar/Ga with $\theta_i=55°$ and $E_i=6$ kJ/mol for a surface temperature of 586 K. Data are open circles; data with fractions of the equilibrium cosine distribution subtracted are filled circles. Theoretical calculations are the solid curve.

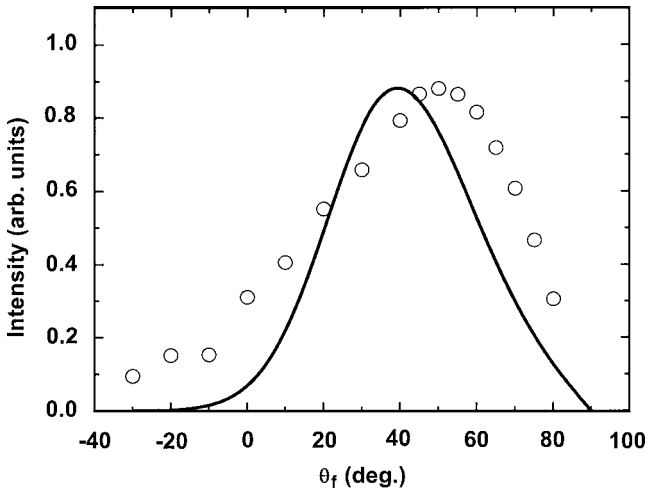

FIG. 6. In-plane angular distribution spectrum for Ne/Ga at a surface temperature $T_S=436$ K with $\theta_i=55°$ and $E_i=6$ kJ/mol. Data are circles and the calculation is the solid curve.

case of Fig. 3, the position and widths of the peaks at all measured temperatures are reasonably well explained.

Figure 5 shows an energy-resolved distribution at the same low energy of $E_i=6$ kJ/mol=63 meV with $\theta_i=\theta_f=55°$ and a surface temperature of 586 K. The calculations for $D=60$ meV are shown as a dashed curve, and the solid curve is calculated for $D=0$. The calculations do not fit the low-energy part of the data, which may be due to a trapping-desorption component which is not calculated. A trapping-desorption component might be expected since the estimated well depth is comparable to the incident energy.

B. Neon and xenon on gallium

Figures 6 and 7 show examples of angular distributions for neon and xenon scattering from liquid gallium at a surface temperature of 586 K with $E_i=6$ kJ/mol and $\theta_i=55°$. For Ne/Ga of Fig. 6, no fraction of a Knudsen distribution was subtracted from the data, a well depth $D=10$ meV was included in the interaction potential, and $v_R=900$ m/s. This well depth is somewhat smaller than the typical value for Ne adsorption on a range of other metal surfaces where it is measured or estimated to be of the order of 30 meV.[18,19] The agreement of calculations with the data for Ne/Ga in Fig. 6 is not as good as most of the angular distributions. Subtracting a small Knudsen distribution from the data does not result in a better agreement. This implies that if trapping-desorption processes are the reason for this disagreement, and such processes are likely because of the low incident energy, they result in a nonequilibrium (noncosine) component to the scattering. However, the qualitative agreement for Ne/Ga implies that predominantly direct scattering processes are involved in the collision, as has been noted previously for Ne scattering from many metal surfaces.[1]

For Xe scattering, the diffuse component was dominant and the subtracted equilibrium fraction measured temperatures were 96% at 308 K, 92% at 436 K, and 90% at 586 K.

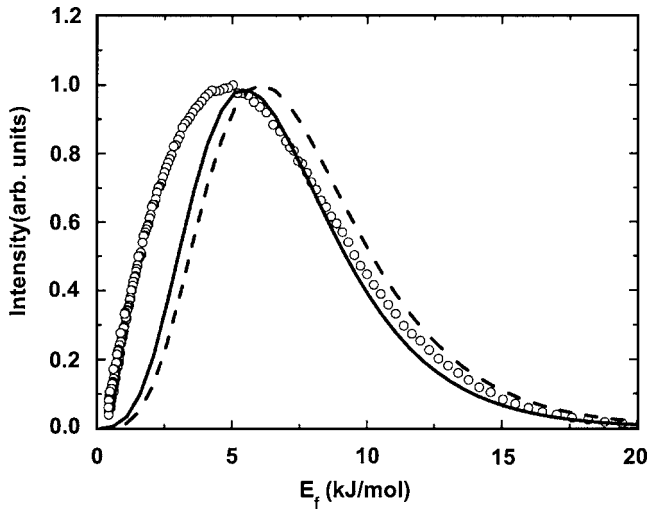

FIG. 5. Energy-resolved spectra for Ar/Ga for $E_i=6$ kJ/mol, $T_S=586$ K, and $\theta_i=\theta_f=55°$. Calculations for $D=60$ meV are the dashed curve, calculations for $D=0$ are the solid curve, and data are open circles.

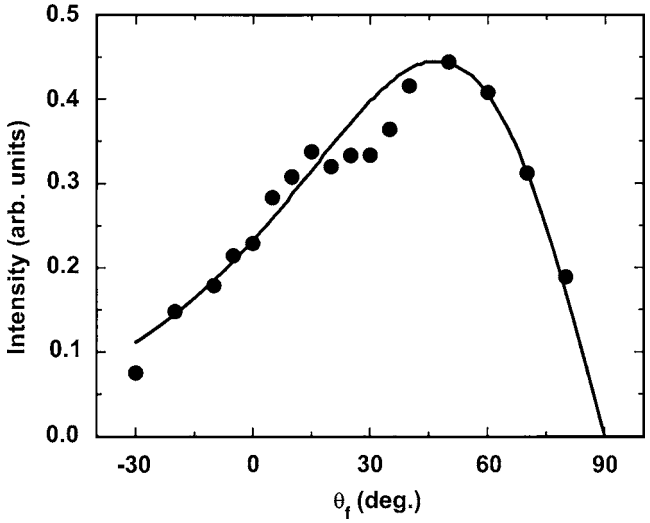

FIG. 7. In-plane angular distribution spectrum for Xe/Ga for surface temperature $T_S=586$ K with $\theta_i=55°$, $E_i=6$ kJ/mol, $v_R=300$ m/s, and an interaction well depth of 100 meV. Data, after subtraction of an equilibrium component, are shown as filled circles, and the calculation is the solid curve.

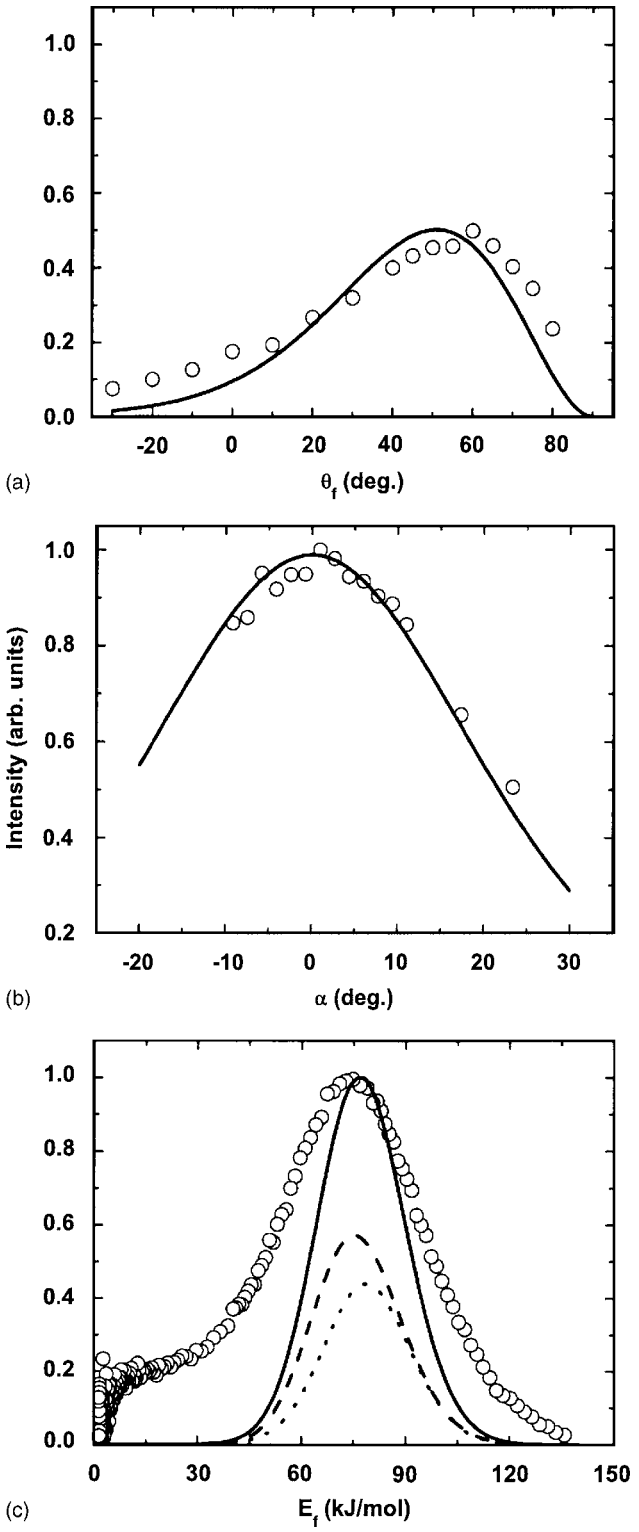

FIG. 8. In-plane, out-of-plane, and energy-resolved spectra for Ar/Bi: (a) In-plane spectra angular distribution with $\theta_i=55°$, $E_i=92$ kJ/mol, and $T_S=586$ K. (b) Out-of-plane angular distribution for $\theta_i=55°$, $E_i=92$ kJ/mol, and $T_S=586$ K. (c) Energy-resolved spectrum for $\theta_i=\theta_f=55°$, $E_i=95$ kJ/mol, and $T_S=573$ K, with the theory curves as in Fig. 1. Data are open circles.

The well depth was chosen as 100 meV and $v_R=300$ m/s. This value for the interaction potential well depth is in basic agreement with results for Xe adsorption on many metal surfaces, as determined from measurements of sticking coefficients and heats of adsorption,[18–20] in which D ranges approximately from 100 to 300 meV.

For both Ne and Xe, just as for Ar, an effective mass of 1.65 Ga atoms was used. As in the case of Ar scattering, the widths and positions of the large, broad peaks are in reasonable agreement with measurements. For the case of Xe, the data exhibit a small shift in the most probable final angle toward the surface normal with increasing temperature that is well explained by the calculations. For the case of Ne, a similar shift is predicted by the theory, but a somewhat smaller shift appears in the measurements.

C. Argon on bismuth

High-energy angular distributions and an energy-resolved spectrum for argon scattering from liquid bismuth are presented in Fig. 8. The in-plane and out-of-plane angular distributions are for an energy of 92 kJ/mol and an incident angle of 55°, while the energy-resolved data are for the slightly higher energy of 95 kJ/mol with both incident and final angles fixed at 55°. The calculations are shown as solid curves, with the single and double scattering contributions denoted as in Fig. 1. The value of $v_R=350$ m/s. In this case, the surface effective mass is taken to be the same as a single Bi atom, and the agreement between theory and measurement is equally good as obtained for the Ar/Ga case.

Figure 9 gives an in-plane angular distribution and an energy-resolved spectrum for a low-energy 6 kJ/mol beam of Ar scattering from liquid Bi. The calculations for the in-plane angular distributions are the same as for Fig. 8 above, except that in this case calculations for three different well depths are presented, $D=0$, 10, and 100 meV. The relatively small well depth of 10 meV gives a reasonable agreement with the energy-resolved spectrum. In the angular distribution, calculations with the smaller well depth do not explain the rather large intensity in the neighborhood of θ_f near the surface normal, but this discrepancy may be due to the presence of an equilibrium $\cos\theta_f$ component,[1] which was not subtracted from the data in Fig. 9.

D. Argon on indium

Examples of all three types of scattering distributions for argon scattering from liquid indium at the higher incident energy are shown in Fig. 10. As in previous work on this system,[6,7] the theory, with $v_R=450$ m/s, explains the in-plane data reasonably well, and it is seen that this holds true also for the out-of-plane angular distribution.

Figure 11 shows additional data and calculations for angular distributions taken at $T_S=436$ K and three different energies. The calculations for the lowest energy of 6 kJ/mol include a potential well with $D=100$ meV. The in-plane angular distributions on the left hand side of Fig. 11 are the same as those presented previously[7] and are shown here for completeness.

E. Neon on indium

Figure 12 shows all three types of scattering distributions for the case of neon on indium at low energy. The temperature is $T_S=436$ K, $E_i=6$ kJ/mol, $\theta_i=55°$, and the out-of-plane distribution was taken at a final in-plane polar angle also of 55°. The calculations, shown as solid curves,

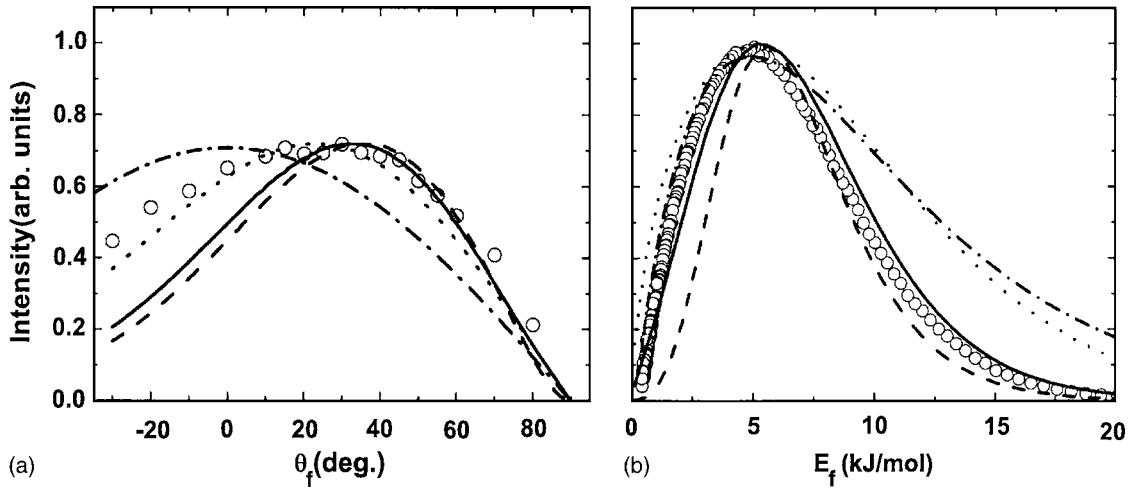

FIG. 9. In-plane and energy-resolved spectra for Ar/Bi for E_i=6 kJ/mol and T_S=586 K: (a) in-plane angular distribution for θ_i=55°; (b) energy-resolved spectrum for $\theta_i=\theta_f$=55°. Data are circles. Theory with well depth zero are the dashed curves, theory with well depth 10 meV are the solid curves, and theory with well depth 100 meV are the dotted curves. A Knudsen distribution is shown in each panel as the dash-dot curve.

used v_R=800 m/s and a well depth D=20 meV. Also shown in the energy-resolved spectrum of Fig. 12(c) is a calculation for D=0, and the calculation with D=20 meV is in significantly better agreement with experiment. The in-plane angular distribution of Fig. 12(a) is in qualitative agreement with the data in a manner similar to the low-energy case of Ne/Ga in Fig. 6, and again the same explanation for the lack of a quantitative agreement may apply.

IV. DISCUSSION AND CONCLUSIONS

A classical theory of atomic scattering from surfaces has been used to analyze newly available data[1,5] for the rare gases Ne, Ar, and Xe scattering from liquid metal surfaces. Previously, it has been shown that such theories can do a reasonable job of describing the observed features of rare gas scattering from surfaces,[6,7] but the newly available data provide the opportunity to test the theory over a much wider range of scattering systems and initial conditions. Additionally, the new data include measurements of angular distributions out of the plane of scattering, providing data from a region of phase space that has not been investigated before. One major difference with the theoretical approach taken here is that all scattering is described with a single consistent model. In the previous work, total intensity angular distributions were calculated with the smooth surface model[7] of Eq. (1), while energy-resolved intensity spectra were calculated with a different classical expression which is more appropriate for a surface of discrete scattering centers.[6]

The energy range over which measurements were made was quite large, from 6 to 100 kJ/mol, while the incident and final angles for energy-resolved and out-of-plane measurements were always in the neighborhood of the specular position with θ_i=55°. In general, the comparisons of theory with the measurements were good, especially for the higher incident energies. A good agreement was obtained with the new, out-of-plane measurements.

The theoretical expression of Eq. (1) predicts that the FWHM of the energy-resolved spectra should increase very nearly with the square root of the surface temperature, and this is clearly seen in Fig. 2.

For the gases Ar and Xe at the low incident energy of 6 kJ/mol, there was a diffusive component in the scattered intensity that could be associated with trapping and subsequent desorption from the attractive physisorption well. This component was particularly strong for Xe scattering. Upon assuming that the trapping-desorption fraction escapes with an equilibrium Knudsen flux distribution at the surface temperature, the present theoretical comparisons are in good agreement with measurements

At low energies, the physisorption well of the potential not only gives rise to trapping and desorption, but it can also have a significant effect on both the angular and energy-resolved scattering distributions largely because of the refraction of the projectile toward a more normal incidence angle and its increased energy as it collides with the surface inside the well. In the present theory, the physisorption was modeled by a square well which is adequate for describing the refraction and enhanced energy in classical scattering. Comparisons with the data at low incident energies provide predictions of well depths for many of the gas-metal combinations, and these results are presented in Table I. Although no direct experimental measurements exist for the physisorption well depths for these combinations of rare gases and liquid metals, the values obtained here are quite reasonable with the possible exception of Ar/Bi and are of the same order of magnitude as well depths for the same rare gases measured or predicted for other metal surfaces.[18–20] For the case of Ar on Bi, the well depth value of 10 meV was obtained from the calculations for the energy-resolved data of Fig. 9(b). This value seems small in comparison with expected values of well depths for Ar interacting with metal surfaces. In fact, the comparison of calculations with the angular distribution of Fig. 9(a) would indicate a larger well depth that could be as large as 100 meV.

The authors of Ref. 1 made the interesting suggestion that differences in surface tension may be the cause of some

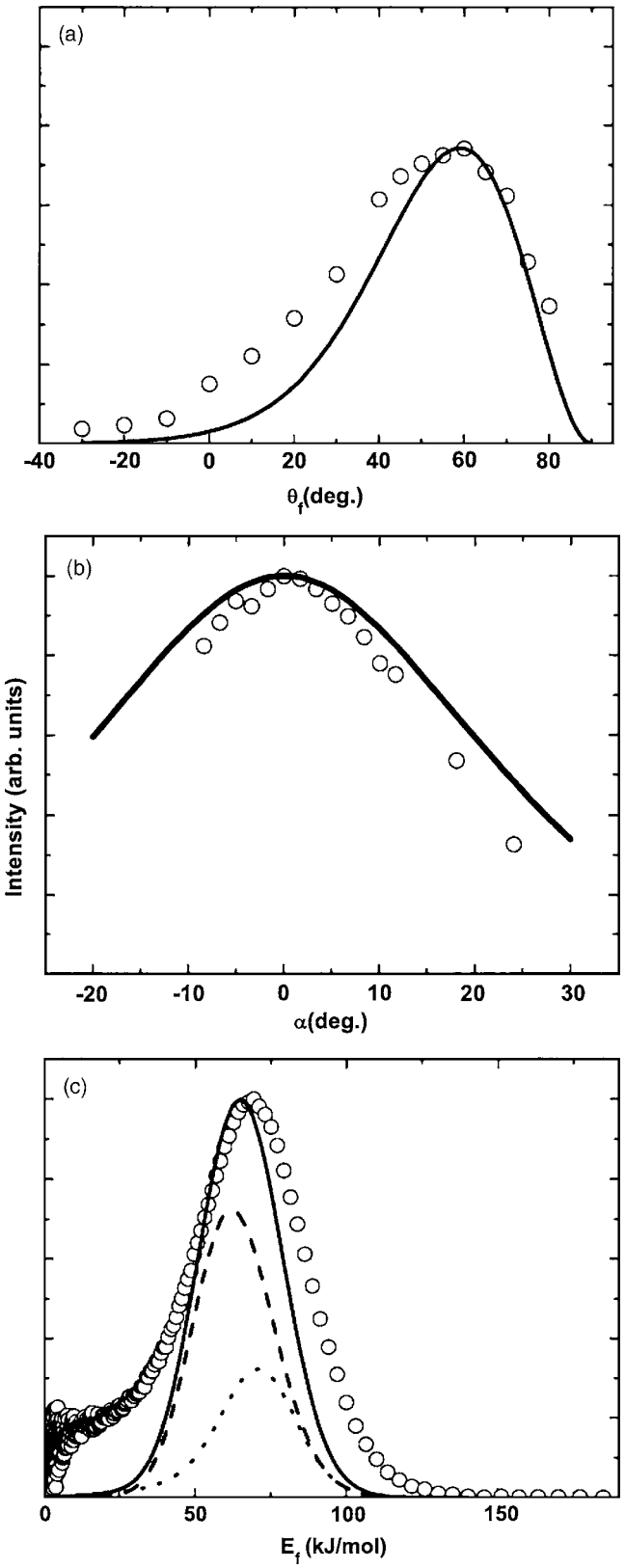

FIG. 10. Ar/In: (a) in-plane angular distribution and (b) out-of-plane angular distribution, both for $\theta_i=55°$, $E_i=92$ kJ/mol, and $T_S=586$ K. (c) Energy-resolved spectrum for $\theta_i=\theta_f=55°$, $E_i=95$ kJ/mol, and $T_S=436$ K.

of the features observed in the scattering spectra. In particular, for the case of Ar angular distributions, they observed that the peak in-plane scattered intensity decreased with the order Ga > In > Bi, and the corresponding peak widths increased with the same ordering. Since this is also the order of decreasing strengths of the surface tensions of the three liquids, they argued that a larger surface tension resulted in a flatter surface, hence a sharper and narrower scattered angular distribution. The present calculations fail to produce the observed ordering in the Ar angular distributions. In fact, the calculated order of the peak intensities is exactly the reverse, i.e., they decrease in the order Bi > In > Ga, and this behavior can be ascribed to the differences in the liquid atom masses. It is possible to calculate the correct ordering, but only with v_R parameter choices that are quite different from those used here.[1] However, these different parameter values do not give rise to the relatively good agreement with all of the scattered spectra shown here.

It is possible to assign a correlation length to the collision through the Gaussian-type term in parallel momentum transfer of Eq. (1), which can be regarded as having a decay length R_C whose value is given by $R_C=\hbar v_R/\sqrt{2k_BT_S\Delta E_0}$.[24] The length R_C is proportional to v_R, and it might be considered of interest to try to relate surface tensions to such a correlation length, especially since for the present calculations the v_R parameters for Ar (and hence the correlation lengths) decrease in the order Ga > In > Bi, the same as the ordering of the surface tensions. However, for all cases considered here, the correlation lengths are very short, less than the average spacing between liquid atoms. Thus, it is unlikely that the present calculations can lend support to arguments based on differences in surface tension. The theory used here is based on a description of the scattering process that involves collisions with only one liquid atom at a time and is highly localized in time and space, as indicated by the very short correlation lengths. However, this suggests that experiments carried out in the quantum mechanical regime such as low-energy He atom scattering, which would have much larger correlation lengths, might be sensitive to differences in surface tension.

One interesting result observed here in connection with the liquid Ga surfaces is that the energy-resolved spectra for all three rare gases could not be made to agree with measurements unless an effective mass for the surface of 1.65 Ga atoms was used. For In and Bi, the surface mass of a single metal atom was satisfactory. This larger effective mass is suggestive of a collective effect, in which the incoming rare gas pushes on a mass involving more than one metal atom. The presence of such a collective effect seems to be supported by independent measurements that show that Ga, in contrast to In and Bi, exhibits an unusually large amount of quasiordered layering in the liquid state, and this layering persists to relatively large temperatures.[11]

There remains the question of whether this collective effect involves atoms in layers of the liquid beneath the surface, or whether it is with other atoms in the surface layer. Interestingly, another metallic surface examined with atomic and molecular scattering has also required a larger effective mass. This is Ru(0001), where considerable data are available for the scattering of Ar (Ref. 21) and N_2 (Ref. 22) under incident energy and angular conditions similar to those used here. For both of these systems, in order to obtain agreement between the data and calculations similar to those considered

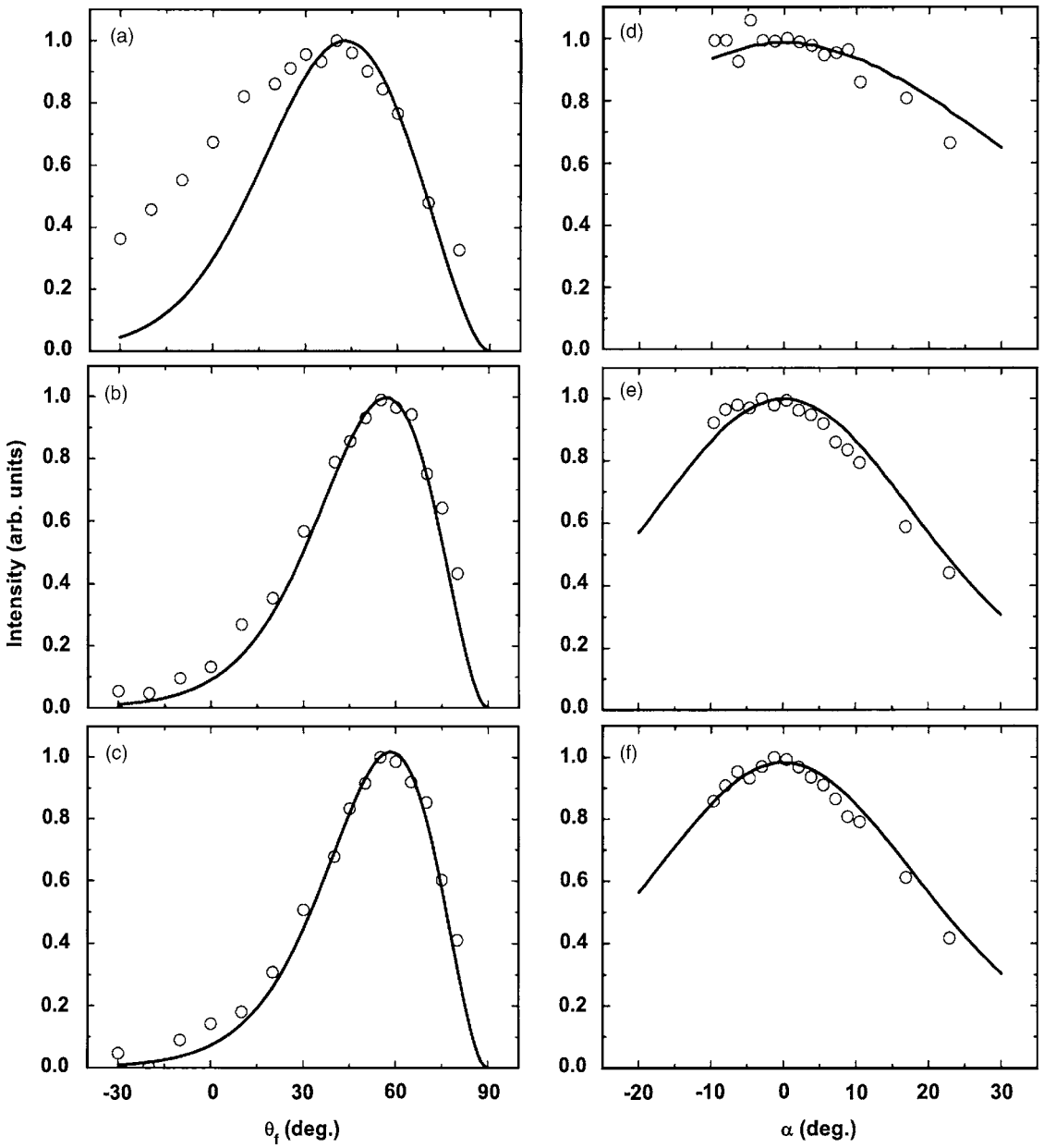

FIG. 11. Angular distributions for Ar/In for θ_i=55°, T_S=436 K, and three different incident energies of (a) 6 kJ/mol, (b) 42 kJ/mol, and (c) 92 kJ/mol. On the left are in-plane angular distributions and on the right are out-of-plane distributions measured starting from the in-plane polar angle θ_f=55°. Data are open circles and calculations are solid curves.

here, it was necessary to choose an effective mass for the Ru surface that was larger than two Ru atomic masses.[23,24]

Interestingly, the experiments on N_2/Ru(0001) were able to make independent measurements of the energy associated with normal and parallel motions of the scattered molecules. Comparisons of calculations with these measurements indicated that the collective effect in that system was with Ru atoms in layers beneath the surface, and not with multiple atoms in the surface layer. Unfortunately, the present rare gas scattering experiments were not taken over a large enough range of initial and final angles to permit investigation of this dependence in the liquid metals. In order to examine the spatial dependence of the effective mass effect, the ideal experiments would be to contrast measurements made with near-normal incident and final angles with measurements made at grazing incident and final angles. It would also be possible to explore this more fully using angular combinations in which one of the two angles θ_i and θ_f was alternately located near normal with the other angle close to surface grazing conditions.

One could raise the question of whether detailed calculations, such as molecular dynamics simulations carried out with more realistic and reliable potentials of the molten metal surfaces, could reveal more information about the mass dependence. Two such studies of Ar scattering from molten metal surfaces have already been reported, one using Lennard-Jones potentials[3] and the other using embedded atom potentials,[4] but the calculated angular distributions and energy-resolved spectra were no better than those obtained with the methods used here. It is doubtful that atom scattering experiments in the classical, multiphonon regime such as those considered here will be able to adequately sort out the

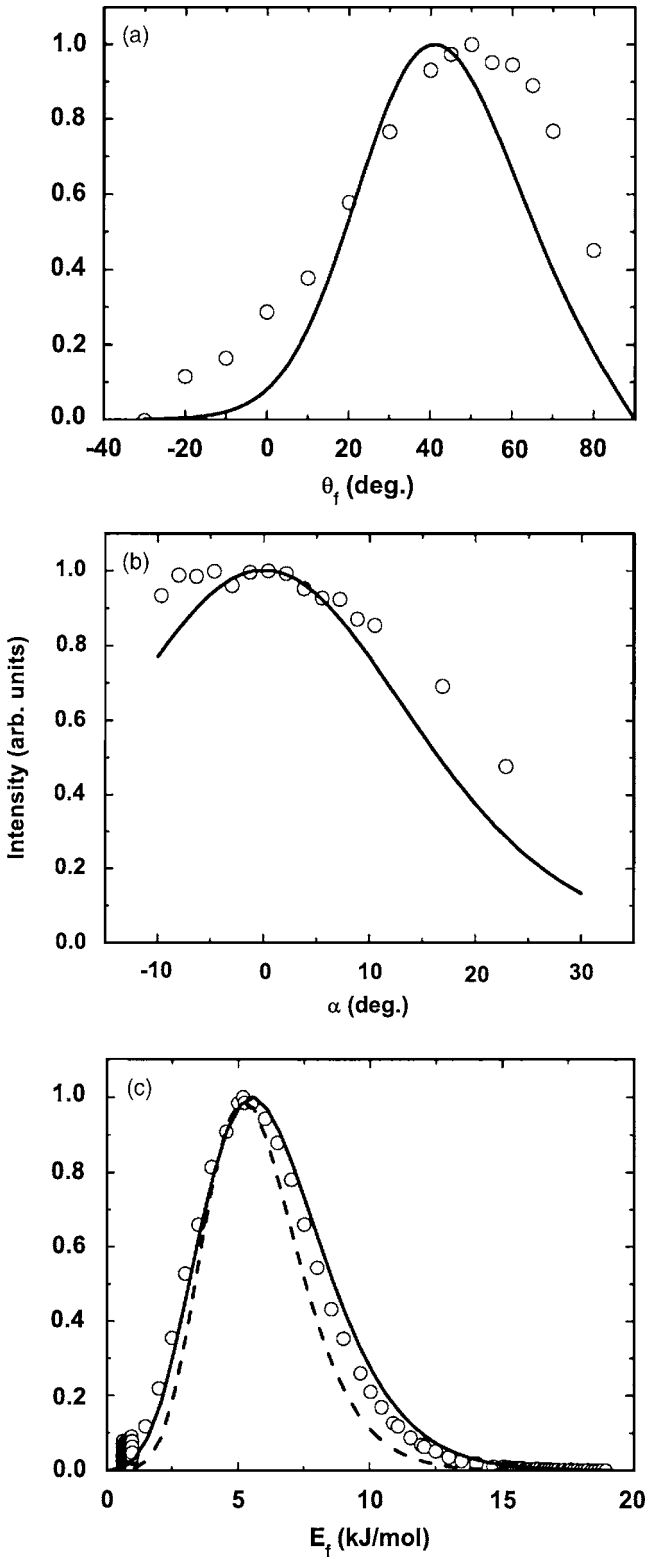

FIG. 12. Ne/In distributions for E_i=6 kJ/mol, θ_i=55°, and T_S=436 K. (a) In-plane angular distribution, (b) out-of-plane angular distribution, and (c) energy-resolved spectrum for θ_f=55°, showing calculation for D=0 meV with a dashed curve; all other calculations are for D=20 meV shown as solid curves.

microscopic origins of the effective mass. This would be better addressed through experiments capable of measuring single quantum excitations of vibrational modes such as inelastic He atom scattering or electron energy loss spectroscopy (EELS). Comparisons of theoretical calculations with inelastic scattering spectra using reliable potentials should reveal details of the mass dependence and should also reveal the importance of surface tension, especially if evidence for surface capillary waves could be found.

TABLE I. Table of well depths that could be estimated by comparisons with the data, in dimensions of meV.

	Ga	In	Bi
Ne	10	20	···
Ar	60	100	10
Xe	100	···	···

There is also a second reason for suggesting experiments over a large range of incident and final angles, and this has to do with the determination of the velocity parameter v_R. This parameter is completely defined in terms of a weighted average over all phonon modes parallel to the surface. Thus, measurements of v_R could, in principle, provide useful information about the surface phonon spectral density and, hence, about the dynamics of the atoms at the liquid surface. It has been pointed out that a much better way of determining accurate values of v_R would be through comparisons of calculations with experimental data taken, first at nearly specular conditions such as is the case in the experiments considered here, and then compared with measurements taken at angles that differ significantly from specular conditions.[25]

ACKNOWLEDGMENTS

We would like to thank G. M. Nathanson, Jason Morgan, and David Castro for helpful discussions and for making their data available to us. This work was supported by the U.S. Department of Energy under Grant No. DE-FG02-98ER45704.

[1] M. Manning, J. Morgan, D. Castro, and G. M. Nathanson, J. Chem. Phys. **119**, 12593 (2003).
[2] W. R. Ronk, D. V. Kowalski, M. Manning, and G. Nathanson, J. Chem. Phys. **104**, 4842 (1996).
[3] L. Tribe, M. Manning, J. Morgan, M. D. Stephens, W. R. Ronk, E. Treptow Gilbert, M. Nathanson, and J. L. Skinner, J. Phys. Chem. B **102**, 206 (1998).
[4] D. Chase, M. Manning, J. Morgan, G. Nathanson, and R. Benny Gerber, J. Chem. Phys. **113**, 9279 (2000).
[5] J. A. Morgan and G. M. Nathanson, J. Chem. Phys. **114**, 1958 (2001).
[6] A. Muis and J. R. Manson, J. Chem. Phys. **107**, 1655 (1997).
[7] A. Muis and J. R. Manson, J. Chem. Phys. **111**, 730 (1999).
[8] J. Dai and J. R. Manson, J. Chem. Phys. **119**, 9842 (2003).
[9] S. F. Shuler, G. M. Davis, and J. R. Morris, J. Chem. Phys. **116**, 9147 (2002).
[10] B. Scott Day, S. F. Shuler, A. Ducre, and J. R. Morris, J. Chem. Phys. **119**, 8084 (2003).
[11] M. J. Regan, E. W. Kawamoto, S. Lee, P. S. Pershan, M. Maskil, M. Deutsch, O. M. Magnussen, B. Ocko, and L. E. Berman, Phys. Rev. Lett. **75**, 2498 (1995).
[12] M. J. Regan, P. S. Pershan, O. M. Magnussen, B. M. Ocko, M. Deutsch, and L. E. Berman, Phys. Rev. B **54**, 9730 (1996).
[13] H. Tostmann, E. DiMasi, P. Pershan, B. Osko, O. G. Shpyrko, and M. Deutsch, Phys. Rev. B **59**, 783 (1999).
[14] T. Scopigno, R. Di Leonardo, L. Comez, A. Q. R. Baron, D. Fioretto, and G. Ruocco, Phys. Rev. Lett. **94**, 155301 (2005).
[15] R. Brako and D. M. Newns, Phys. Rev. Lett. **48**, 1859 (1982); R. Brako, Surf. Sci. **123**, 439 (1982).

[16] H.-D. Meyer and R. D. Levine, Chem. Phys. **85**, 189 (1984).
[17] J. R. Manson, Phys. Rev. B **43**, 6924 (1991).
[18] A. R. Miedema and B. E. Nieuwenhuys, Surf. Sci. **104**, 491 (1981).
[19] G. Vidali, G. Ihm, H.-Y. Kim, and M. W. Cole, Surf. Sci. Rep. **12**, 133 (1991).
[20] H. Schlichting, D. Menzel, T. Bruner, and W. Brenig, J. Chem. Phys. **97**, 4453 (1992).
[21] B. Berenbak, S. Zboray, B. Riedmuller, D. C. Papageorgopoulos, S. Stolte, and A. W. Kleyn, Phys. Chem. Chem. Phys. **4**, 68 (2002).
[22] H. Mortensen, E. Jensen, L. Diekhöner, A. Baurichter, A. C. Luntz, and V. V. Petrunin, J. Chem. Phys. **118**, 11200 (2003).
[23] H. Ambaye and J. R. Manson, J. Chem. Phys. **125**, 084717 (2006).
[24] W. W. Hayes and J. R. Manson, Phys. Rev. B **75**, 113408 (2007).
[25] W. W. Hayes and J. R. Manson, Phys. Rev. B **74**, 073413 (2006).